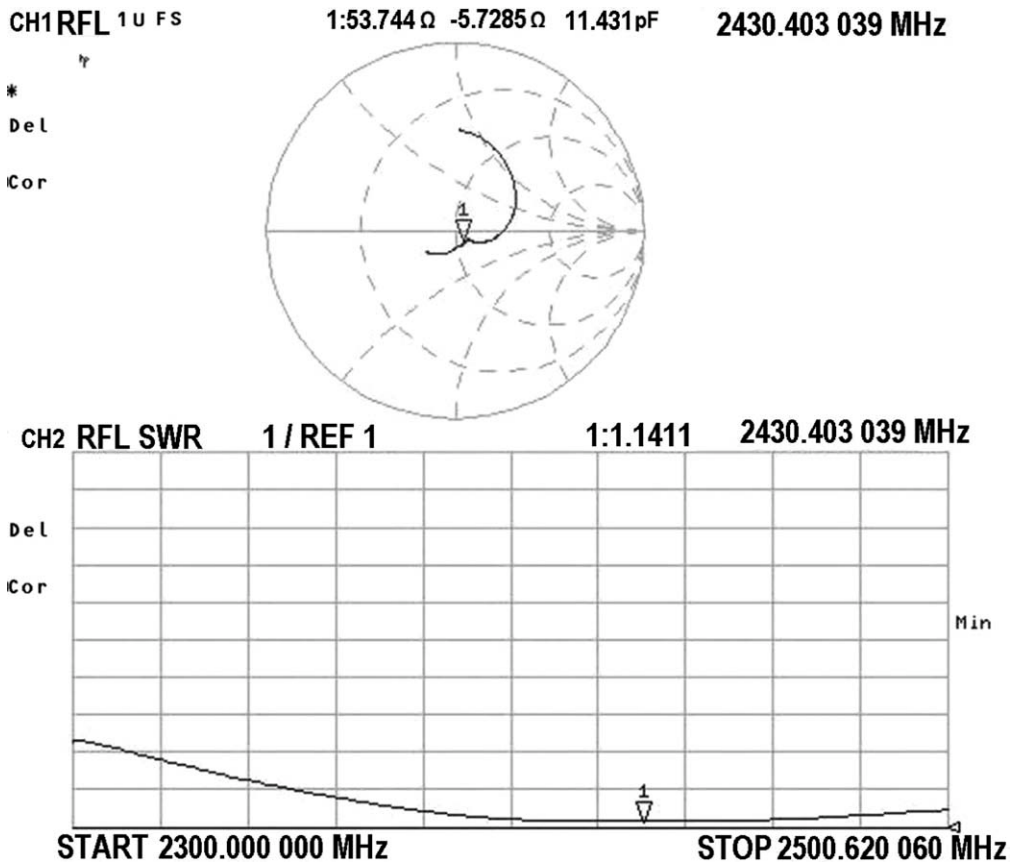

Figure 6 Measured input impedance and VSWR plots for a 3 × 3 space-fed array

measured VSWR was less than 2 from 2.35 to more than 2.5 GHz. At 2.45 GHz, the measured gain of the array was 16 dBi. This was close to the simulated value of 16.1 dBi. The ratio of received power levels with the transmitting antenna vertically and horizontally polarized gives the axial ratio. The measured axial ratio was 0.6 dB at 2.45 GHz.

4. CONCLUSIONS

High-gain circular polarization can be easily obtained using space-fed microstrip antenna arrays without the need for a complex feed network. With the feed patch antenna designed to generate circular polarization, overall gain can be increased by increasing the number of array elements. The design is simple, easy to fabricate, and gives high efficiency and gain with low side lobe levels.

REFERENCES

1. P. Chine and G. Kumar, Three dimensional, efficient, directive microstrip antenna array, In: Proceedings of the IEEE AP-S International Symposium, Washington, DC, 2005, pp. 243–246.
2. G. Kumar and K.P. Ray, Broadband microstrip antennas, Artech House, Norwood, MA, 2003.
3. R. Bhide, Space-fed microstrip antenna arrays, M. Tech Thesis, Indian Institute of Technology Bombay, India, 2009.
4. R. Bhide and G. Kumar, Equivalence of space-fed microstrip antenna array with horn antenna, Microwave Opt Technol Lett, in press.
5. IE3D, version 12.21, Zeland Software, Inc., Fremont, CA, USA.

GENERALIZED NEGATIVE-REFRACTIVE INDEX TRANSMISSION LINE BASED ON DEFECTED GROUND STRUCTURE

Young-Ho Ryu,[1] Jae-hyun Park,[2] Jeong-Hae Lee,[2] and Heung-Sik Tae[2]
[1] School of Electrical Engineering and Computer Science, Kyungpook National University, Seoul 121-791, South Korea
[2] Department of Electronic and Electrical Engineering, Hongik University, Seoul 121-791, South Korea; Corresponding author: jeonglee@hongik.ac.kr

Received 12 January 2010

ABSTRACT: *The planar generalized negative-refractive index transmission line (G-NRI TL) is proposed using only distributed structures, such as defected ground structure, stub with rectangular patch, wire-bonded interdigital capacitor, and short stub. The characteristics, such as dispersion relation and frequency response of the G-NRI TL are analyzed by circuit analysis, full wave simulation, and measurement. The results show a good agreement.* © 2010 Wiley Periodicals, Inc. Microwave Opt Technol Lett 52:2223–2225, 2010; Published online in Wiley InterScience (www.interscience.wiley.com). DOI 10.1002/mop.25467

Key words: *metamaterial; generalized negative-refractive index transmission Line; defected ground structure*

1. INTRODUCTION

Multiband RF devices with superior performance have been developed widely and rapidly for modern wireless communication systems [1]. To comply with the trends, the generalized negative-

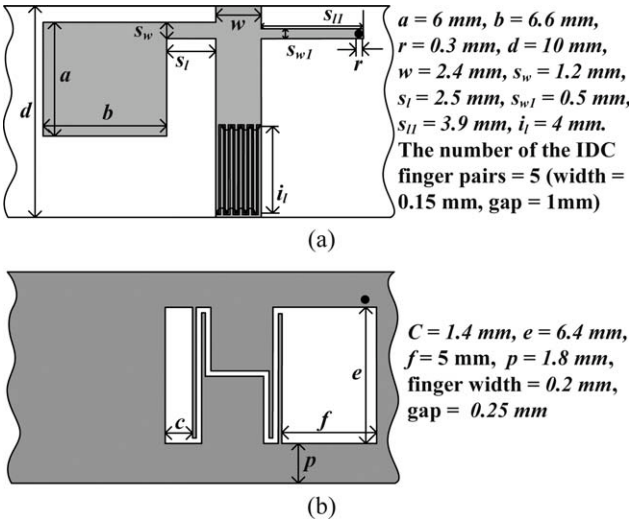

Figure 1 Unit-cell of the proposed G-NRI TL (Substrate: Rogers RT 5880 $-\varepsilon_r = 2.2$, height = 0.787 mm)

refractive index transmission line (G-NRI TL) [2] was presented. The G-NRI TL has an advantage of multiband applications due to many transmission branches of two right-handed (RH) and two left-handed (LH) branches in Brillouin zone (BZ) [3]. However, the unit cell of G-NRI TL utilized lumped elements in Ref. [2] is large due to the connection part between the lumped elements. The G-NRI TL consisting of lumped elements cannot be used for radiative application since the lumped element based-structure is impractical due to its inability to radiate [4]. In this article, the G-NRI TL using only distributed structures is presented. The balanced conditions of the G-NRI TL for broadband matching are provided, similar to CRLH TLs. The G-NRI TL satisfying the balanced conditions will be designed.

2. DESIGN AND ANALYSIS OF G-NRI TL

Figure 1 shows the proposed unit cell of the G-NRI TL. The unit cell consists of a defected ground structure (DGS), a stub with rectangular patch, a wire-bonded interdigital capacitor (WBIDC), and a short stub by a metallic via. The DGS and the stub with a rectangular patch are equivalently modeled as an impedance with parallel *LC* resonant circuit (C_d, L_d) [5] and an admittance with series *LC* resonance circuit (C_p, L_s), respectively, as shown in Figure 2. The WBIDC and the short stub are represented by the series capacitance of C_i and the shunt inductance of L_v, respectively. To complete an equivalent circuit, the capacitance of C_t and the inductance of L_t, parasitic RH components of the host TL are added. Consequently, the equivalent circuit of the G-NRI TL is completed, as shown in Figure 2. In Figure 2, the series impedance (Z), shunt admittance (Y), and characteristic impedance (Z_C) of the G-NRI TL can be derived as

$$Z(\omega) = j\omega L_t \frac{\omega^2\omega_h^2 - \left(\omega_1^2 - \omega^2\right)\left(\omega_d^2 - \omega^2\right)}{\omega^2\left(\omega_d^2 - \omega^2\right)}, \tag{1a}$$

$$Y(\omega) = j\omega C_t \frac{\omega^2\omega_v^2 - \left(\omega_2^2 - \omega^2\right)\left(\omega_s^2 - \omega^2\right)}{\omega^2\left(\omega_s^2 - \omega^2\right)}, \tag{1b}$$

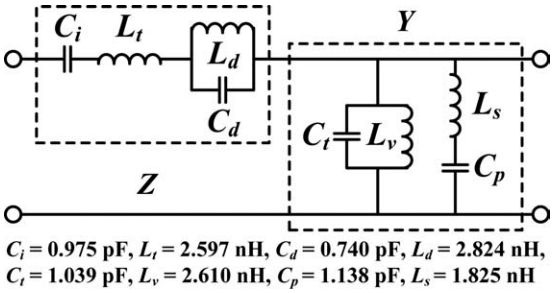

Figure 2 Equivalent circuit of G-NRI TL

$$Z_c(\omega) = \sqrt{\frac{L_t}{C_t}}\sqrt{\frac{\omega^2\left(\omega_s^2 - \omega^2\right)\left[\omega^2\omega_h^2 - \left(\omega_1^2 - \omega^2\right)\left(\omega_d^2 - \omega^2\right)\right]}{\omega^2\left(\omega_d^2 - \omega^2\right)\left[\omega^2\omega_v^2 - \left(\omega_2^2 - \omega^2\right)\left(\omega_s^2 - \omega^2\right)\right]}} \tag{2}$$

where,

$$\omega_1 = \frac{1}{\sqrt{C_i L_t}},\ \omega_2 = \frac{1}{\sqrt{C_t L_v}},\ \omega_d = \frac{1}{\sqrt{C_d L_d}},\ \omega_s = \frac{1}{\sqrt{C_p L_s}},$$
$$\omega_h = \frac{1}{\sqrt{C_d L_t}},\ \text{and}\ \omega_v = \frac{1}{\sqrt{C_t L_s}}.$$

The effective permeability and permittivity values are obtained from $\mu_{\text{eff}} = Z(\omega)/j\omega d$ and $\varepsilon_{\text{eff}} = Z(\omega)/j\omega d$, respectively [3]. The balanced conditions for broad-band matching are directly obtained from (2) as follows: $\omega_1 = \omega_2$, $\omega_d = \omega_s$, and $\omega_h = \omega_v$. If the balanced conditions are satisfied, then the impedance matching can be achieved because the characteristic impedance is the same with that of the host TL as seen in (2). In the equivalent circuit, each parameter is extracted from the circuit and full wave simulations (Ansoft's Designer and HFSS) when the G-NRI TL satisfies the balanced conditions. According to the open- and short-ended boundary conditions (BCs), the ZOR frequencies of the G-NRI TL are calculated by the following equations [6]:

Open-ended BC:

$$\omega_{\text{GZOR1,2}}^2 = 0.5(\omega_2^2 + \omega_s^2 + \omega_v^2) \pm 0.5\sqrt{(\omega_2^2 + \omega_s^2 + \omega_v^2)^2 - 4\omega_2^2\omega_s^2)} \tag{3a}$$

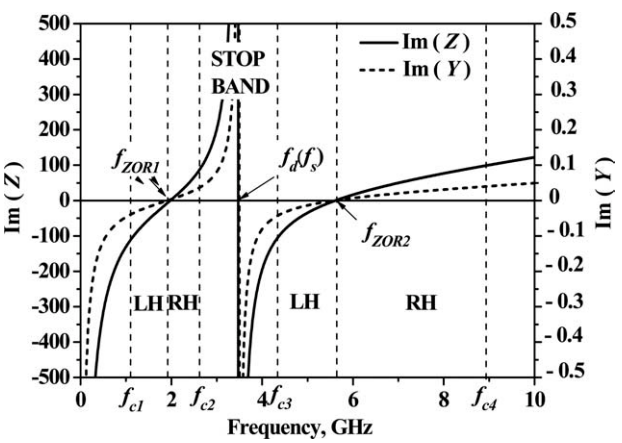

Figure 3 Imaginary values of Z and Y

Short-ended BC:

$$\omega^2_{GZOR1,2} = 0.5(\omega_1^2 + \omega_d^2 + \omega_h^2) \pm 0.5\sqrt{(\omega_1^2 + \omega_d^2 + \omega_h^2)^2 - 4\omega_1^2\omega_d^2}. \quad (3b)$$

Form (3), it is found that the G-NRI TL inherently has two ZOR frequencies, which are independent of the total length (Nd) of resonators.

3. SIMULATED AND MEASURED RESULTS

Figure 3 shows the imaginary values of the impedance (Z) and admittance (Y) in Figure 2, corresponding to the $\omega d\mu_{\text{eff}}$ and $\omega d\varepsilon_{\text{eff}}$, under the balanced conditions. The ω_d (ω_s) of 3.47 GHz (3.50 GHz), ω_{ZOR1} of 1.91 GHz, and ω_{ZOR2} of 5.60 GHz are directly calculated by (1) and (3), respectively. In Figure 3, the whole frequency range can be divided by the critical frequency points of f_{c1}, f_{ZOR1}, f_{c2}, f_{c3}, f_{ZOR2}, and f_{c4}. Each bounded region is characterized, according to the signs of the Im(Z) and Im(Y), by RH or LH band. These cutoff frequencies of f_{c1} (1.15 GHz), f_{c2} (2.71 GHz), f_{c3} (4.31 GHz), and f_{c4} (9.54 GHz) are calculated using the dispersion relation [3] with the condition that βd is equal to π.

Figure 4 shows the dispersion curves that are obtained by full wave simulation and theory. The theoretical result is in good agreement with that of the simulation. Four transmission bands are simulated as follows: the first LH band, the first RH band, the second LH band, and the second RH band are from 1.15 to 1.87 GHz, from1.87 to 2.71 GHz, from 4.31 to 5.68 GHz, from 5.68 to 9.54 GHz, respectively. Figure 5 shows the simulated and measured s-parameter of 2-stage G-NRI TL. Four transmission bands in two-stage GMTL case are measured as follows: the first LH band, the first RH band, the second LH band, and the second RH band are from f_{c1} (1.36 GHz) to f_{ZOR1} (1.95 GHz), from f_{ZOR1} to f_{c2} (2.69 GHz), from f_{c3} (4.56 GHz) to f_{ZOR2} (5.71 GHz), from f_{ZOR2} to f_{c3} (9.70 GHz), respectively. These measured results are in agreement with the results, which are obtained from the theoretical dispersion curves in Figure 4. It is directly known that the G-NRI TL has an advantage of the multiband applications because the dispersion curve has more transmission branches in BZ (up to10.84 GHz). The proposed

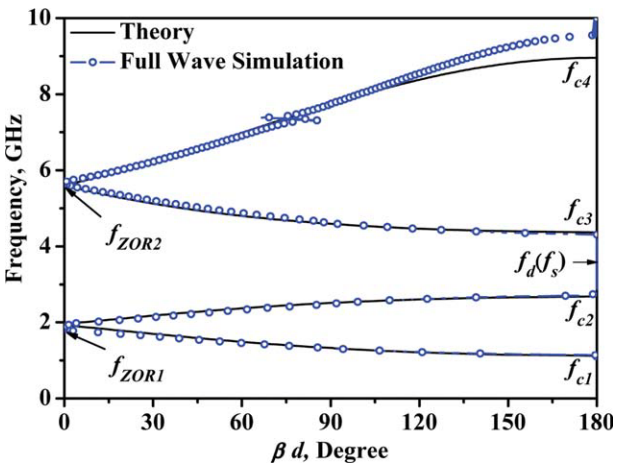

Figure 4 Theoretical and simulated dispersion curves of G-NRI TL. [Color figure can be viewed in the online issue, which is available at www.interscience.wiley.com]

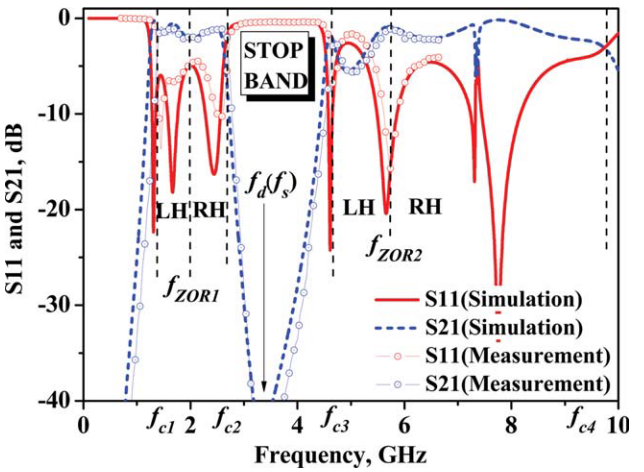

Figure 5 Frequency response of G-NRI TL. [Color figure can be viewed in the online issue, which is available at www.interscience.wiley.com]

G-NRI TL is compact because the series resonance part is made by DGS. It also does not require the connected part between the components. The length of the unit cell (0.163 λ_g) is reduced by 37.8% in compassion with that (0.262 λ_g) of Ref. [2] at the f_{ZOR1}. In addition, the TL can be used for the radiative applications because the TL consists of only distributed structures. Therefore, it is expected that the G-NRI TL can be applied to multiband RF devices, such as dual-band ZOR antennas, multiband power dividers, multiband filters, and so on.

4. CONCLUSION

The G-NRI TL consisting of only distributed structures is proposed. It can be utilized for the radiative application. The dispersion relation and frequency behavior of the G-NRI TL are analyzed by theory, simulation, and measurement, showing good agreement.

ACKNOWLEDGMENT

This work was supported by grant No. 2007-KRF-314-D00188 from the Korea Research Foundation.

REFERENCES

1. Y.X. Guo, M.Y.W. Chia, and Z.N. Chen, Miniature built-In multiband antennas for mobile handsets, IEEE Trans Antennas Propag 52 (2004), 1936–1944.
2. M. Studniberg and G.V. Eleftheriades, Physical implementation of a generalized NRI-TL medium for quad-band applications, Proceedings of 37th International Conference on EuMA, Germany, 2007.
3. G.V. Eleftheriades and K.G. Balmain, Negative-refraction metamaterials: Fundamental principles and applications, 1st ed., IEEE Press, New York, NY, 2005.
4. A. Lai, K.M.K.H. Leong, and T. Itoh, Infinite wavelength resonant antennas with monopolar radiation pattern based on periodic structures, IEEE Trans Antennas Propag 55 (2007), 868–876.
5. D. Ahn, J.S. Park, C.S. Kim, J. Kim, Y. Qian, and T. Itoh, A design of the low-pass filter using the novel microstrip defected ground structure, IEEE Trans Microwave Theory Tech 49 (2001), 86–93.
6. A. Sanada, C. Caloz, and T. Itoh, Planar distributed structures with negative refractive index, IEEE Trans Microwave Theory Tech 52 (2004), 1252–1263.